Chapter 2
Application of Solar Distillation Systems with Phase Change Material Storage

S. K. Shukla

Abstract This chapter presents the analysis of a solar distillation system with phase change material storage system. There is always a scarcity of clean and pure drinking water in many developing countries. Water from various sources is often brackish (i.e. contain dissolved salts) and/or contains harmful bacteria and therefore, cannot be used for drinking purpose. In addition, there are many coastal areas where seawater is abundant but potable water is not available in sufficient quantity. Apart from drinking purpose, pure water is also useful for health and industrial purposes such as hospitals, schools and batteries etc. Many parts of India, particularly, rural areas, coastal areas and many urban areas too, have a major drinking water problem. Sufficient drinking water, at accepted purity level, is just not available.

2.1 Introduction

Contaminated drinking water is one of the reasons of major health hazards responsible for almost 90 % of the health problems in rural areas. Women and children are mostly affected because they are quite vulnerable to water borne diseases. Generally, women are responsible for fulfilling the requirement of water in their household and thus, spend their large chunk of time for procuring the same. Out of 40–50 litres per capita per day (lpcd) of water requirement for domestic consumption, only 2 lpcd is the drinking water. A total amount of 5–10 lpcd water is needed for drinking and cooking purposes and thus, it is only this quantity of water that needs to meet the stringent quality standards of potability prescribed by W.H.O. or other similar agencies, whereas the remaining amount of water needed for washing and cleaning can be of intermediate quality. Intensive use of chemical fertilizers in agriculture and enhanced Industrial

S. K. Shukla (✉)
Department of Mechanical Engineering, I.I.T (B.H.U.),
Varanasi, U.P. 221005, India
e-mail: skshukla.mech@itbhu.ac.in

J. P. Davim (ed.), *Modern Mechanical Engineering*, Materials Forming, Machining and Tribology, DOI: 10.1007/978-3-642-45176-8_2,

activities cause the natural and inorganic pollutants to leach down to underground sub surface water and hence, the drawing of water through Hand-Pumps may not remain safe for drinking purpose. Keeping in view the poor paying capacity of people, water supply to remote areas through pipeline could be uneconomical and moreover, it also encourages wasteful use of high quality water in washing, cleaning and toiletries. Therefore, for economical and sustainable water management system, it is important to supply water at appropriate level of quality, which is suitable enough for the kind of use for which it is meant [29–33].

Water and energy are two inseparable items that govern our lives and promote civilization. Looking into the history of mankind one finds that water and civilization were also two inseparable entities. It is not a coincidence that all great civilizations were developed and flourished near large bodies of water. Rivers, seas, oases and oceans have attracted mankind to their coasts because water is the source of life. The transportation of drinking water from far-off regions is usually not economically feasible/desirable, desalination of available brackish water has been considered as an alternative approach. Conventional desalination processes based on distillation involve phase change. These are multistage flash distillation (MSF), multieffect distillation (MED) and vapor compression (VC), which could be thermal VC or mechanical VC. MSF and MED processes consist of a set of stages at successfully decreasing temperature and pressure. MSF process is based on the generation of vapors from seawater or brine due to a sudden pressure reduction when seawater enters to an evacuated chamber. The process is repeated stage by stage at successively decreasing pressure. This process requires an external steam supply, normally at temperature around 100 °C. The maximum temperature is limited by the salt concentration to avoid scaling and this maximum limits the performance of the process. On MED, vapors are generated due to the absorption of thermal energy by the seawater. The steam generated in one stage or effect is able to heat the salt solution in the next stage because next stage is at lower temperature and pressure. The performance of the process is proportional to stages or effects. MED plants normally use an external steam supply at temperature about 70 °C. On TVC and MVC, after initial vapor is generated from the saline solution, this vapor is thermally or mechanically compressed to generate additional production. On the other hand the membrane processes such as reverse osmosis (RO) and electro-dialysis (ED) do not involve phase change. The first one require electricity or shaft power to drive the pump that increase the pressure of saline solution to that required. This required pressure depends on the salt concentration of the resource of saline solution, which is normally around 70 bar for sea water desalination. Both of them RO and ED (membrane processes) are used for brackish water desalination whereas distillation is applicable to the entire range of salinities up to seawater. In fact it is the only process, which removes with certainty any organisms (bacteria, viruses and also pyrogens) contained in feed water. Theoretically distillation is capable of removing all non-volatile matter. In practice, however, some carryover of dissolved and colloidal matter into the distillate may take place. End product purity expressed in specific conductivity is between 4.0 and 0.066 μg/cm at 25 °C, depending upon the technique used.

Since the cost of heat plays a decisive role in various distillation processes, viz., single stage, multistage distillation, flash distillation and vapor compression distillation; it seems advantageous to harness the heat of the sun for this purpose. Over a period of 100 years several types of solar stills have been designed and tested. There has been a significant progress in the field of solar distillation during the past four decades, perhaps, due to the general increase of interest in solar energy utilization. Because of cost free energy and low operating cost, as there are no moving parts involved in these systems, the solar distillation shows a comfortable economic advantage over other seawater distillation processes. Further, solar distillation requires simple technology and less maintenance so that it can be used at any rural place. Thus, in order to capture this very advantage of distillation process, cost effective Solar Stills have been designed and developed. And they have proved their performance and cost effectiveness.

When drying foods, the key is to remove moisture as quickly as possible at a temperature that does not seriously affect the flavor, texture and color of the food [1]. If the temperature is too low in the beginning, microorganisms may grow before the food is adequately dried. If the temperature is too high and the humidity is too low, the food may harden on the surface. This makes it more difficult for moisture to escape and the food does not dry properly. Although drying is a relatively simple method of food preservation, the procedure is not exact.

For the preservation of these agricultural products, the convective hot air drying using fossil fuels/grid-electricity is the most common technique employed in commercial dryers around the globe. However, due to unreliable or too expensive for the farmer to utilize them, more emphasis is being paid to solar energy as an alternative source for such applications [2]. In addition, it has tremendous potential especially in several regions of the world, where this source is abundantly available. In past four decades, various types of solar dryers have been designed, developed and tested with the aim of achieving faster drying of food product at a minimum cost. Ekechukwu and Norton [3] presented a comprehensive review on design, construction and operation of different types of solar dryers. However, all these dryers can be broadly grouped into three major types as direct, indirect and mixed mode, depending on arrangement of system components and mode of solar heat utilization [4]. The operation of these dryers is primarily based on the principle of natural or forced air circulation mode. In many rural regions of developing countries, the farmers have been preferably adopting natural convection over forced mode operated dryer, since it is inexpensive to construct and easy to operate without the need of grid connected electricity and supplies of other non-renewable sources of energy. In addition, natural convection cabinet dryer of direct type has been popular among farmers especially in India because of its ability for drying 10–15 kg fruits and vegetables at household level [5, 6]. Selection of solar dryer for a particular food product is primarily governed by quality requirements and economic factors. The common practice in predicting performance of solar energy system is to solve a set of several inter-related steady state heat balance equations representing various components [7–9].

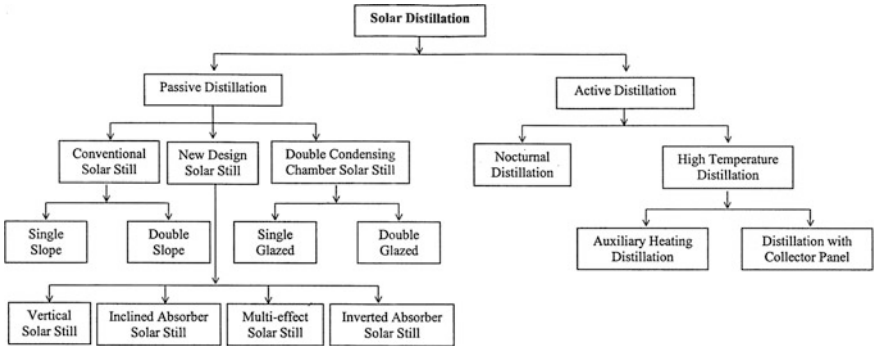

Fig. 2.1 Classifications of solar stills

2.1.1 Solar Distillation

Solar distillation uses the heat of the sun directly in a simple piece of equipment to purify water. The equipment, commonly called a solar still, consists primarily of a shallow basin with a transparent glass cover. The sun heats the water in the basin, causing evaporation. Moisture rises, condenses on the cover and runs down into a collection trough, leaving behind the salts, minerals, and most other impurities, including germs. Although it can be rather expensive to build a solar still that is both effective and long-lasting, it can produce purified water at a reasonable cost if it is built, operated, and maintained properly. The classification of solar distillation process is given in Fig. 2.1.

2.1.2 Basin Type Solar Still

A basin type solar still is a simple device for obtaining potable water from contaminated or saline water using solar energy. Such a solar still is shown in Fig. 2.2. It consists of a blackened tray containing saline water, covered with a sloping glass roof. The collection troughs are attached at the lower edges of the glass covers. The water condenses on the inner surface of the glass cover, flows into the collection troughs due to gravity. The pure water is removed as product.

The main energy flows in the basin type solar still have been shown in the flow chart Fig. 2.3. Solar energy, which is transmitted by the glass cover and absorbed by the water and the blackened tray, heats the water in the basin. This absorbed energy conducted through the haze; radiated, or convected to the glass cover, or is carried by evaporation of water to the glass cover. The cover is substantially transparent to solar radiation and opaque to infrared radiation and serves as a condenser for the saturated vapour within the still. The glass cover transfers heat to the surroundings; by radiation to the sky and by convection to the ambient air.

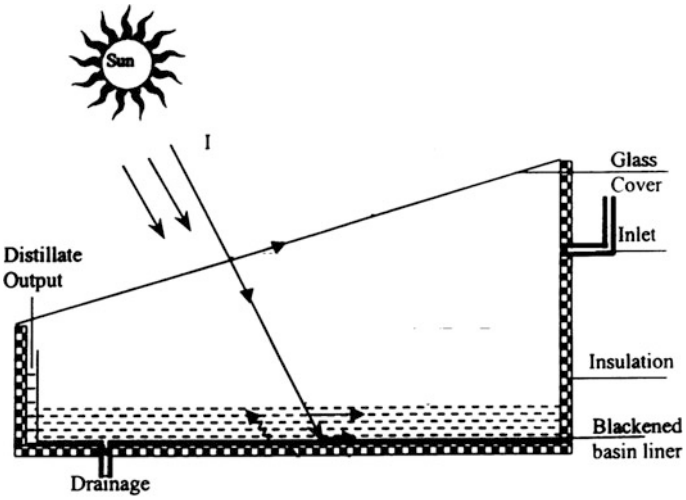

Fig. 2.2 Single basin solar still

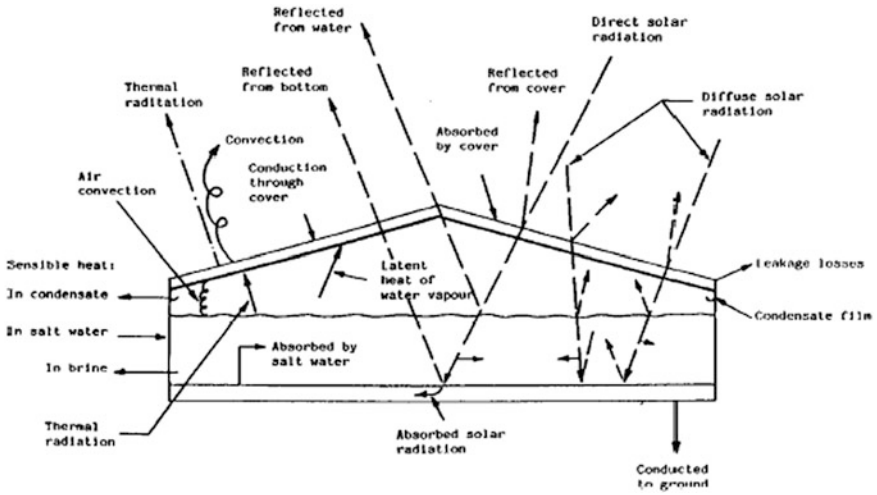

Fig. 2.3 Energy flow diagram

The basin type solar stills have been covered in the textbooks [9, 10]. The constructional and operational features of still have been described in the technical literature [9–20]. These features of the still are summarized by Dunkle [15]. A basin type solar still may be erected directly on dry ground, or well insulated at the bottom by a suitable insulating material. To cut down heat losses from sides and edges suitable insulation may be provided around the basin. However, it has been pointed out that the heat losses to the ground are small in case of larger basins even

when uninsulated [10, 14, 15]. Cooper [16] has explained that for large stills most of the heat conducted into the ground during the day is conducted back during the night. Malik et al. [10] have carried out a periodic heat transfer analysis and concluded that ground and edge losses are only 2 % of the incident energy.

2.1.3 Efficiency of the Still

If Q_t (in Joules/m^2 day) is the amount of solar energy incident on the glass cover of a still and Q_e (in Joules/m^2 day) is the energy utilised in vaporizing water in the still, then the daily output of distilled water M_e (in kg/m^2 day) is given by

$$M_e = \frac{Q_e}{l} \tag{2.1}$$

where l (in Joules/kg) is the latent heat of vaporization of water. The efficiency of the still is given by $\frac{Q_e}{Q_t}$. An ideal still is considered to be a still with zero conductive heat losses and with zero heat capacities of water, glass and insulation. Cooper [16] has shown that efficiency of such a still as high as 60 % for high values of solar insolation.

2.1.4 The Basic Heat Transfer Modes in a Solar Still

The physics of solar stills is mainly a superposition of heat and mass transfer by molecular diffusion and buoyant convection and of radiative heat exchange between the surrounding surfaces. The latter is practically independent from the foregoing two, but these are very complex processes, whose components must not be investigated separately.

The operation of a solar still is governed by various heat transfer modes, convection and radiation being the prominent ones. Free convection accompanied by evaporative mass transfer and radiation are modes of heat transfer between the water surface and the glass cover inside the still. The coefficient of heat transfer is corporated in Nusselt number which is related to the Grashof and Prandtl numbers as,

$$N_u = f(G_r.P_r)$$

$$N_u = \frac{h_{cw}.x}{k_f}$$

$$G_r = x^3.\rho_f^2.g.\beta'.\Delta T \Big/ \mu_f^{\,2} \tag{2.2}$$

$$P_r = \frac{C_p.\mu_f}{k_f}$$

In the case of a still x, the characteristic dimension of the system is the distance between the surface of water and the glass cover.

The steady state performance of a basin type solar still can be predicted following the solar energy textbooks (Malik et al. [10] Duffie and Beckman, [9]). The textbooks have recommended Dunkle's [15] heat transfer model which has been in the technical literature for some time. This heat transfer model is described below. The basic heat transfers in a still can be grouped into two categories:

(a) Inner heat transfer (between the water surface and the glass cover):

The basic heat transfer modes between the water surface and the glass cover are convection, radiation and evaporation. The radiative, convective, and evaporative heat transfer coefficient between water surface and glass cover (Dunkle [15]) are given below assuming water surface and glass cover as two infinite parallel plates.

(i) The radiative heat transfer coefficient,

$$h_{rw} = \frac{\sigma\left[(T_w + 273)^4 - (T_g + 273)^4\right]}{\left(\frac{1}{\varepsilon_g} + \frac{1}{\varepsilon_w} - 1\right)(T_w - T_g)} \tag{2.3}$$

and rate of heat transfer by radiation is expressed as

$$Q_{rw} = h_{rw}(T_w - T_g)$$

(ii) The heat transfer between the water surface and glass cover is by free convection. The convective heat transfer coefficient,

$$h_{cw} = 0.884\left[(T_W - T_g) + \frac{(P_w - P_g)(T_w + 273)}{(268.9 \times 10^3 - p_w)}\right]^{1/3} \tag{2.4}$$

and rate of convective heat transfer is expressed as

$$Q_{cw} = h_{cw}(T_w - T_g)$$

Dunkle [15] made use of the relation between Nusselt number and Grashof number for turbulent convection in a horizontal enclosed air space. The buoyancy term in Grashof number is modified by the density effect due to composition (due to evaporation) as well as temperature based in part on experiments with the evaporation of water into quiescent air [19]. Malik et al. [10] have explained the mathematical development. The correlation assumes that the air is saturated with water vapour at the temperature of water in the basin and at the temperature of glass cover.

(iii) The evaporative heat transfer coefficient,

$$h_{ew} = \frac{9.15 \times 10^{-7} h_{cw}(P_w - P_g)h_{fg}}{(T_w - T_g)} \tag{2.5}$$

is based on the relation between mass transfer and heat transfer, assuming a Lewis number 1.0.

(b) Outer heat transfer (between the glass cover and the environment):

(i) The radiative heat transfer coefficient between glass cover and the "sky" (atmosphere) is given by,

$$h_{rg} = \sigma \varepsilon_g \left(T_g^2 + T_s^2\right)\left(T_g + T_s\right) \tag{2.6}$$

where T_s is the apparent (effective) temperature of the atmosphere which acts as the sink for radiative heat transfer.

(ii) Bottom and Edge Heat Transfer

The heat is also transferred or loss from water in ambient through the insulation and subsequently convection/radiation of the bottom or side surface of the box. Hence the bottom loss can be written as

$$U_b = \left[\frac{1}{K_i/L_i} + \frac{1}{h_{cb} + h_{rb}} + \frac{1}{h_w}\right] \tag{2.7}$$

where L_i, K_i, h_{rb}, h_{cb} and h_w are thickness, thermal conductivity of the insulation, radiative and convective heat transfer coefficients from bottom to ambient and the convective heat transfer coefficient between basin liner of the still and the water. However last two terms in the above expression do not contribute significantly and the heat loss can be considered only through conduction from bottom,

$$U_b = K_i/L_i \tag{2.8}$$

Similarly edge loss is also mainly by conduction through the insulation and can be written as

$$U_e = \frac{U_b.A_e}{A_b} \tag{2.9}$$

where A_b, A_e are bottom and edge areas of the still.

(iii) The convective heat transfer coefficient due to wind,

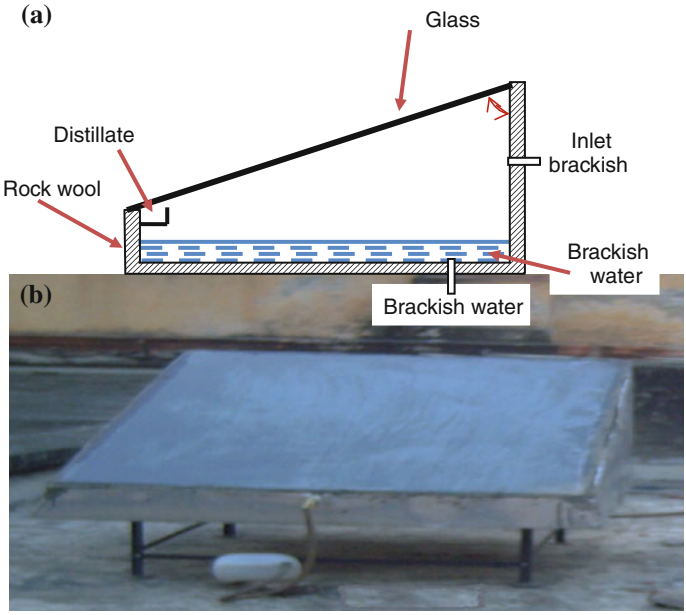

Fig. 2.4 **a** Schematic diagram of passive solar still. **b** Photograph of passive solar still

For calculating the convection losses from the glass cover to the ambient air, wind heat transfer coefficient, may be expressed as a linear function of wind velocity [9]. However, as pointed out by Shukla et al. [12, 13] the heat transfer coefficient in natural environment can be larger by a factor of two or three.

2.2 Design of Solar Stills with Phase Change Material Storage

2.2.1 Conventional Solar Stills

A schematic diagram and photograph of the solar still is given in Fig. 2.4., installed at Renewable Energy Laboratory, Indian Institute of Technology, Banaras Hindu University, Varanasi, India. The basin is fabricated from black painted 2 mm thick mild steel having an area of 1 m^2 each. A vertical gap beneath the horizontal portion of the basin liner is provided to upload and/or unload the PCM through a PVC pipe which takes care of the volumetric expansion of the melting PCM as well. The operational and melting temperature of PCM, in fact, governs the applicability of different types of PCMs. The myristic acid relates to the class of fatty acids that have superior properties, such as, melting congruency, better chemical stability

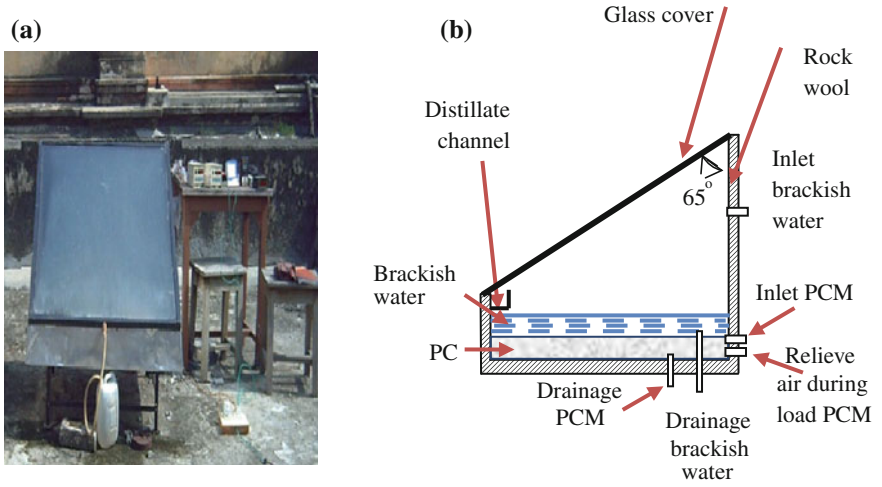

Fig. 2.5 A photograph of solar stills with PCM (**a**) A schematic diagram of the single slope-single basin solar still with the PCM (**b**)

non-toxicity and better thermal reliability over many other PCM [17–19] Schematic diagram and photograph of the conventional single slope solar still are shown in Fig. 2.4a, b, respectively.

2.2.2 Solar Still with Phase Change Material (Myristic Acid) Storage

A photograph and a schematic diagram of the single slope solar still with phase change material (PCM) as a storage medium, is given in Fig. 2.5. The basin, fabricated from a black painted mild steel sheet of thickness 2 mm, has an area of 1 m^2 each.

A vertical gap (0.05 m) beneath the horizontal portion of the basin liner is provided to upload and/or unload the PCM through a pipe which takes care of the volumetric expansion of the melting PCM as well. The operational and melting temperature of PCM, in fact, governs the applicability of different types of phase change materials. The bottom and sides of the basin are insulated by 5 cm thick layer of rock wool contained in an aluminium tray. The top cover of the still is made up of 4 mm thick window glass which inclines at an angle of 25° with horizontal, and has an average transmissivity (τ) of value 0.88. A U-shaped channel is used to collect the condensate from the lower edge of glass cover and carry it to storage. A temperature scanner (Altop Industries ltd, Sn.1005164, model ADT 5003) with resolution 0.1 °C and HTC DT-8811Infrared thermometer range: −20 to 450 °C Spectral response: 6–14 μm CE ASCO products had been used to

record the temperature with k-type thermocouples in solar stills. The solar radiation was measured by using the daystar meter Watts/m^2 ASCO products, the wind speed was observed by HTC Instruments AVM-07 Anemometer vane probe CE.

2.2.3 Energy and Exergy in a Solar Still with PCM

The energy and exergy of solar still with PCM are:

The energy and exergy of solar still with PCM are:

The energy efficiency of the solar still is:

$$mew_d = \sum\nolimits_{24hr} mew_h \tag{2.10}$$

$$\eta_{en\_h} = \frac{mew_h \gamma}{\mathrm{A_b} \sum \mathrm{I(t)}*3600} * 100\,\% \tag{2.11}$$

$$\eta_{en\_d} = \frac{mew_d \gamma}{\mathrm{A_b I(t)} * 3600} * 100\,\% \tag{2.12}$$

The exergy balance of solar still with PCM is

$$\sum Ex_{lost} = \sum Ex_{in} - \sum Ex_{out} + \sum W \tag{2.13}$$

The exergy input is represent the exergy from sun

$$\sum Ex_{in} = A_b * I(t) * \left(1 - \frac{4}{3} * \left(\frac{T_a + 273.15}{Ts + 273.15}\right) + \frac{1}{3} * \left(\frac{T_a + 273.15}{Ts + 273.15}\right)^4\right) \tag{2.14}$$

The last term is the exergy of mechanical work. This term is negligible because no work in solar still.

$$\sum W = 0 \tag{2.15}$$

The exergy output or energy useful is due to evaporation heat transfer.

$$\sum Ex_{out} = \sum Ex_{useful} = \sum Ex_{ev} \tag{2.16}$$

The exergy lost in solar still water is given by

$$\sum Ex_{lost} = mw * Cw * (Tw - Ta) * \left(1 - \left(\frac{T_a + 273.15}{Tw + 273.15}\right)\right) \tag{2.17}$$

The second law efficiency as follows:

$$\eta_{EX} = Ex_{output}/Ex_{in} = 1 - Ex_{lost}/Ex_{in} \tag{2.18}$$

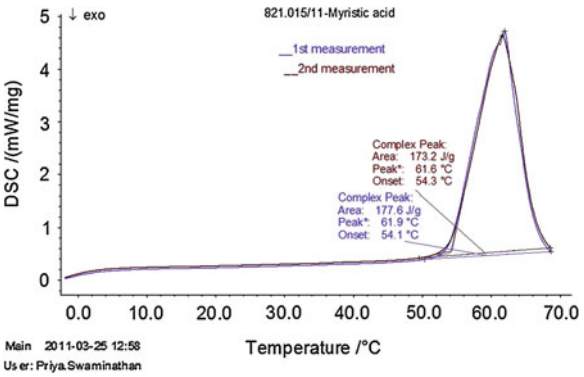

Fig. 2.6 DSC curve for melting temperature and heat of fusion for myristic acid

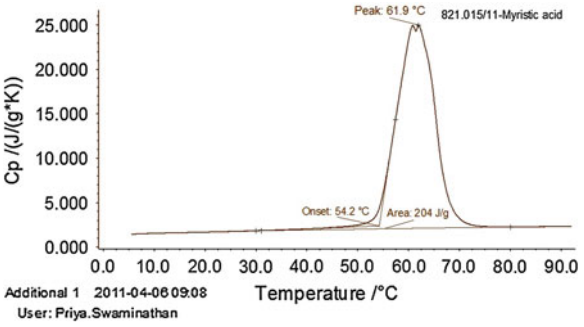

Fig. 2.7 DSC curve for specific heat (Cp) of myristic acid

2.2.4 Selection of Phase Change Material

The measurement of PCM was done in Netzsch Technologies India Pvt Ltd, Chennai, India by using the deferential scanning calorimetry (DSC) technique. The measurements were carried out under the following conditions for the evaluation of melting and heat of fusion as shown in Fig. 2.6:

- Temperature range: 0−80 °C.
- Heating rate: 10 K/min.
- Atmosphere: Static Air.

The measurements conditions of heat capacity of Myristic acid are as follows as shown in Fig. 2.7:

- Temperature range: 0−80 °C.
- Heating rate: 10 K/min.
- Atmosphere: Nitrogen.

The measurements were repeated to check the reproducibility of the results. Therefore, myristic acid, a bye product of milk, has been used as a latent heat storage material due its low cost and easy availability. Table 2.1 summarizes the thermo-physical properties of myristic acid used in the experiment [19–23] (Table 2.2).

Table 2.1 Thermo-physical properties of Myristic acid

S. No	Properties	Value
1.	Melting point	50–54 [°C]
2.	Latent heat of fusion	177 [kJ kg^{-1}]
3.	Thermal conductivity	0.25 [22] [Wm^{-1} $°C^{-1}$]
4.	*Specific heat*	
	Solid at 35 °C	1700 [Jkg^{-1} $°C^{-1}$]
	Liquid at 55 °C	2040 [Jkg^{-1} $°C^{-1}$]
5.	*Density*	
	Solid	990 [kgm^{-3}]
	Liquid	861 [kgm^{-3}]

Table 2.2 Design parameters of solar still with and without PCM

S. No	Parameter	Values, units
1.	A_b	1 [m^2]
2.	A_g	1.1 [m^2]
3.	α_b	0.95
4.	α_g	0.05
5.	α_w	0.05
6.	R_g	0.05
7.	h2	5.7 + 3.8 v, [Wm^{-1} $°C^{-1}$]
8.	K_g	0.035 [Wm^{-2} $°C^{-1}$]
9.	L_g	0.004 [m]
10.	R_w	0.05
11.	ε_g	0.95
12.	ε_w	0.95
13.	m_w	30–50 [kg]
14.	m_{pcm}	10–30 [kg]
15.	L_{ins}	0.05 [m]
16.	L_b	0.002 [m]
17.	K_b	43 [Wm^{-2} $°C^{-1}$]

2.3 Case Study of a New Design

Schematic diagram and photograph of the new design single slope solar still are shown in Fig. 2.8a, b respectively. The new design solar still and conventional solar still were designed based on the optimum inclination through the year for Varanasi city in India. The major components of this solar distillation system were evaporator, condenser and PCM chamber units. The two sides and back walls are covered with aluminium sheet plate, so these walls serve as the internal reflectors. This solar still forms three basins with saline water. Basin 1 was in the evaporator unit while basins 2 and 3 were stacked inside the condenser unit to recover heat from the first effect (Fig. 2a). Basin 1 of (1 × 1 m) of the test still (AR = 1) was constructed from mild steel sheet (0.002 m thick), painted black on the inner

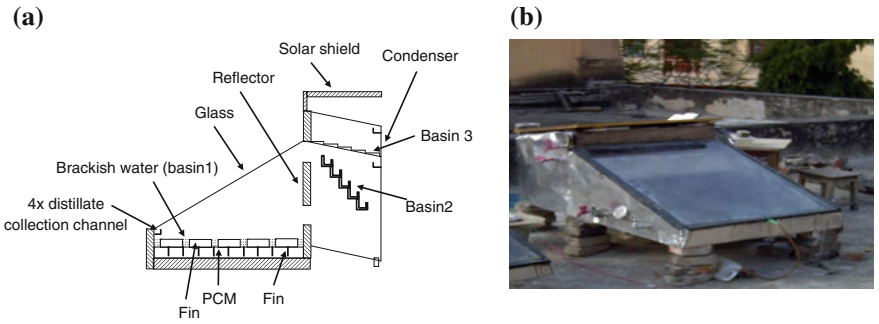

Fig. 2.8 **a** Schematic diagram of new design solar still. **b** Photograph of a new design solar still

Table 2.3 Thermo-physical properties of Lauric acid

S. No	Properties	Value
1.	Melting point	40–43.9 °C
2.	Latent heat of fusion	180 kJ/kg
3.	Thermal conductivity	0.16 Wm^{-1} $°C^{-1}$
4.	*Specific heat*	
	Solid at 25 °C	2.1 $kJkg^{-1}$ $°C^{-1}$
	Liquid at 44 °C	3 $kJkg^{-1}$ $°C^{-1}$
5.	*Density*	
	Solid	1007 kg/m^3
	Liquid	862 kg/m^3

surface to optimize absorption of solar radiation. Basin liners 2 and 3 were made from iron sheet (0.0015 m thick) but they were not painted to reduce resistance to heat conduction. Basin 2 includes stepped basin with 5 steps, with area of 0.3 m^2. While basin 3 was inclined at 12° to enable distillate flow downward into the collection channels. The fins were added in basin 1 of NDSS to decrease the preheating time required for evaporating the still basin water. While using fins in the solar still, the area of the absorber plate increased. Hence, absorber plate temperature and saline water temperature increased. As the temperature difference between water and glass increases, productivity increased. In this work, five circular fins with height and diameter 35, 155 mm, respectively were used. Slender shaped fins were welded on the upper of PCM's chamber. The operational and melting temperature of PCM, in fact, governs the applicability of different types of phase change materials. The lauric acid relates to the class of fatty acids that have superior properties such as melting congruency, good chemical stability and non-toxicity, good thermal reliability over many other PCMs [39, 40]. The Table 2.3 shows thermo-physical properties of Lauric acid. A temperature scanner (Altop Industries ltd, Sn.1005164, model ADT 5003) with resolution 0.1 °C has been used to record the temperature with k-type thermocouples in both system for different location. The solar radiation passes through the glass cover to heat saline

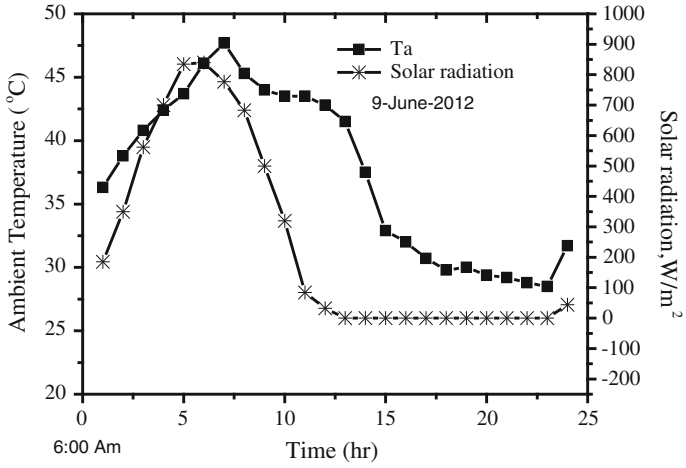

Fig. 2.9 Daily variation of ambient temperature and solar intensity

water in basin 1 (first effect). Then, vapour from the first effect flows upward and condenses when it gets into contact with the inner side of the glass cover at lower temperature while part of the vapour flows into the condensing chamber to heat water in basin 2 (second effect) and basin 3 (third effect). The transfer of water vapour from the still to the condenser could be done through one or more of the following mass transfer modes: diffusion, purging, and natural circulation.

2.4 Result and Discussion

An experimental study during 5th June 2012–18th June 2012 days were carried out to compare the thermal performance of NDSS and CSS. The mass water 10, 15, 20 and 30 kg are used for basin1. The mass water of basin 2 and basin 3 is 4.3 and 7.4 kg respectively. The mass of PCM is varies between 10 to 30 kg for NDSS. The mass water 10, 15, 20 and 30 kg are used for the CSS. Figure 2.9 shows the solar intensity and the hourly yield produced on 9th June 2012.

2.4.1 Temperature of System Components

Figure 2.10 shows the variation of the observed temperature of glass cover (T_{gc}), saline water (T_{wb1}), condenser cover ($T_{co,NDSS}$), glass cover ($T_{gc,CSS}$), saline water ($T_{w,CSS}$) on a 9th June 2012. It is observed that the values of T_{gc} for the CSS ($T_{gc,CSS}$) are higher than those of the NDSS ($T_{gc,NDSS}$) from about 10:00 to 18:00 h, with maximum values of $T_{gc,CSS} = 57$ °C and $T_{gc,NDSS} = 50$ °C.

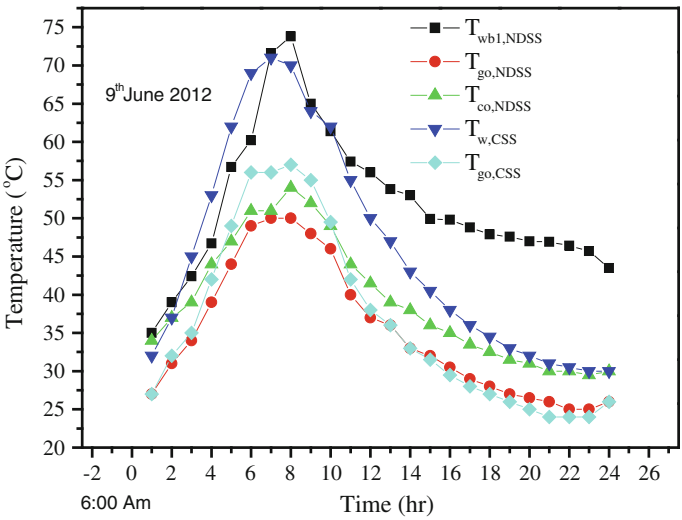

Fig. 2.10 Variation of experimental temperature of saline water in basin1 of CSS and NDSS on 9th June 2012

In addition, the temperature of water in basin for the CSS ($T_{w,CSS}$) is higher than that of the NDSS ($T_{wb1,NDSS}$) from about 8:00 to 13:00 h. But after that the temperature of water in basin for the CSS ($T_{w,CSS}$) is lower than that of the NDSS ($T_{wb1,NDSS}$). It should be mentioned that part of the heat from the evaporator basin flows into the condenser chamber by purging, diffusion and circulation which would tend to lower the glazing temperature of the NDSS [24, 25].

2.4.2 Sunny and Entirely Cloudy Day

An experimental study in sunny and partially cloudy 8th June 2012 and entirely cloudy 7th June 2012 days were carried out to compare the thermal performance of NDSS and CSS. Figure 2.11a, b illustrates the daily productivity of NDSS and CSS in typical sunny and cloudy days, respectively. The mass water of CSS is 20 kg, but for NDSS water masses are 20, 4.3 and 7.4 kg for basin1, basin2 and basin3 respectively.

Figure 2.11a indicates that hourly productivity in NDSS at morning is higher because NDSS has more area of water surface evaporation. But when the height of solar radiation about 9–11am the CSS is reading are higher than NDSS because, some of the absorbed solar energy is used to increase the PCM temperature and the solid fins of basin1, the absorber temperature is higher than the PCM and this trend is inverted in the low solar radiation intensity. It is clear from Fig. 5a, b that the hourly productivity at night is significant for NDSS because of using the stored

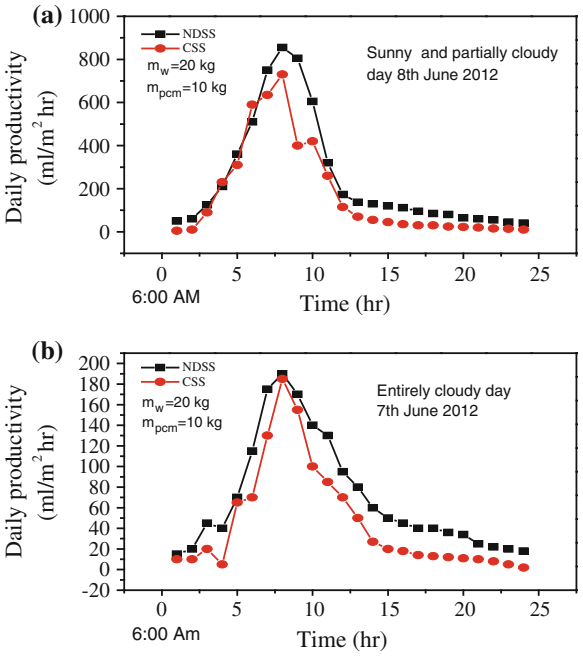

Fig. 2.11 Variations of hourly productivity with time for NDSS and CSS, **a** typical sunny day, 8th June 2012 and **b** entirely cloudy day 7th June 2012

energy. Total productivity for NDSS and CSS is 5710 and 4295 ml/m^2 day for sunny day (8th June 2012) and 1675 and 1095 ml/m^2 day for entirely cloudy day (7th June 2012), respectively. It is also observed that there is a significant difference in the total productivity for the sunny day and entirely cloudy day.

2.4.3 Daytime Productivity

Figures 2.12, 2.13, 2.14 and 2.15 reveals the variation of the daytime productivity with variation the mass of the mass of water 10, 15, 20 and 30 kg for basin1 in the NDSS and for the basin of CSS with 10 kg of PCM. The daytime productivity of CSS is higher than NDSS with 10 kg of water (see Fig. 2.12). The reason of this higher readings of CSS is because the little mass of water (2 cm depth of basin water), thus water immediately is heated and evaporated. But with NDSS the system is gradually heated; part of vapour will circulate inside the integrated condenser. These higher readings of CSS get reduced with mass of 15, 20 and 30 kg, see Figs. 2.12, 2.13 and 2.14. Figure 2.15 shows higher performance of NDSS. Furthermore NDSS yields better results in all figures after 2 pm.

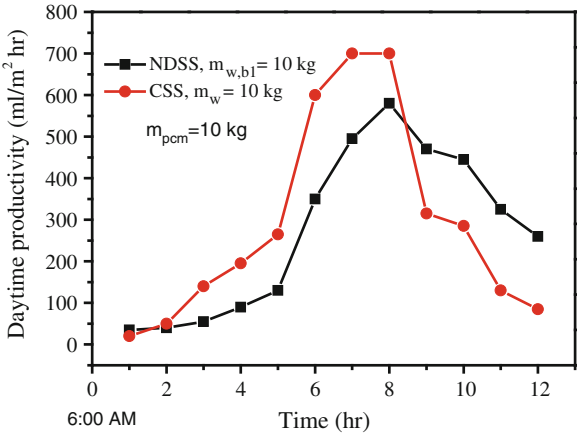

Fig. 2.12 The daytime productivity of NDSS and CSS for $m_{w,b1} = 10$ kg, $m_{pcm} = 10$ kg and $m_w = 10$ kg

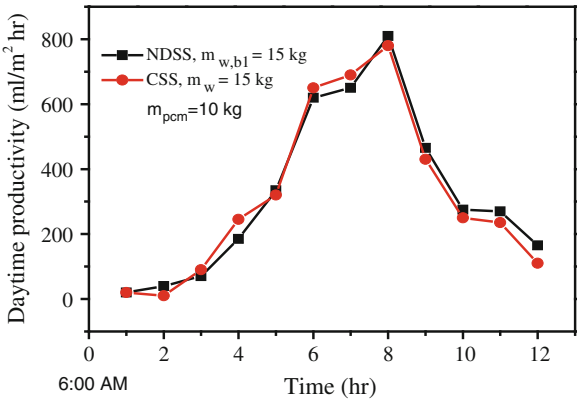

Fig. 2.13 The daytime productivity of NDSS and CSS for $m_{w,b1} = 15$ kg, $m_{pcm} = 10$ kg and $m_w = 15$ kg

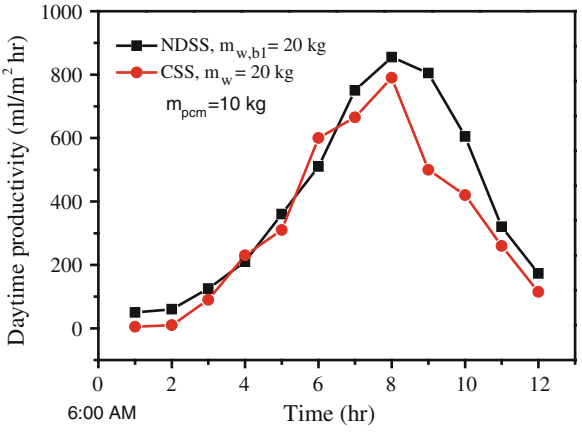

Fig. 2.14 The daytime productivity of NDSS and CSS for $m_{w,b1} = 20$ kg, $m_{pcm} = 10$ kg and $m_w = 20$ kg

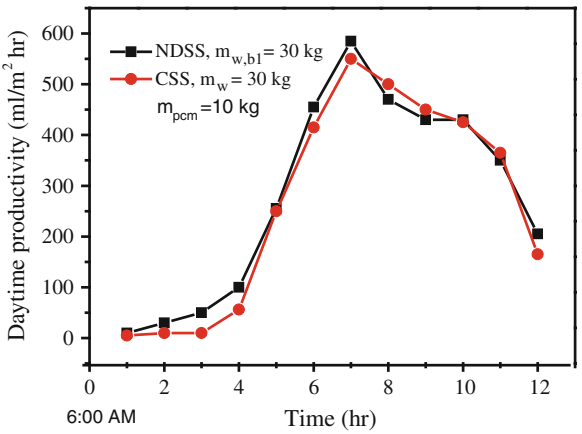

Fig. 2.15 The daytime productivity of NDSS and CSS for $m_{w,b1} = 30$ kg, $m_{pcm} = 10$ kg and $m_w = 30$ kg

2.4.4 Variation of Daytime Productivity with Altered Mass of PCM

Figures 2.16, 2.17 and 2.18 present variations of the daytime productivities with m_{pcm} for different masses of basin1 water $m_{w,b1}$ for NDSS. Assessment of Figures indicated that daytime productivity increases with time. Also the productivity of NDSS of $m_{pcm} = 10$ kg with $m_{w,b1} = 20$ kg is higher value as shown in figures. The reason may be that when the mass of PCM increases, the energy absorbed from basin liner by the PCM increases. Another reason may be the diffusion, purging and circulation inside the integrated condenser increase the convection, evaporating and condensation of vapor water, with the help of the cooler temperature of integrated condenser. The low glass temperature will increase the condensation of water vapor.

2.4.5 Variation of Productivity on Night with Altered Mass of PCM

The key point of using PCM is to increase the productivity at night. Figure 2.19 depicts the influence of adding mass of PCM on the productivity during night time; Productivity increases with the increase of the mass of PCM.

The fluctuation in curves is because the difference in the solar radiation and the cloudy day. Table 2.4 depicts the productivity of 10, 20 and 30 kg of PCMM with 20 kg of water. The difference in productivity for 30 kg PCM with 10 kg PCM is nearly 193 ml/m^2 kg. This value if we compared with the daytime productivity of NDSS that has 20 kg of basin1 water with 10 kg of PCM. But the daytime productivity of NDSS that has 20 kg of basin1 water with 10 kg of PCM is greater

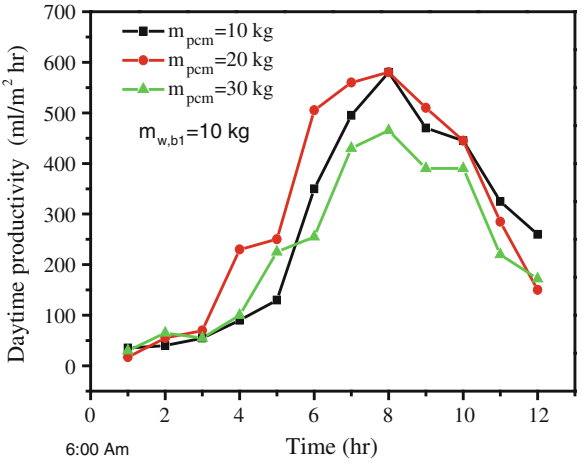

Fig. 2.16 Variation of daytime productivity of NDSS for $m_{pcm} = 10$, 20 and 30 kg with $m_w = 10$ kg

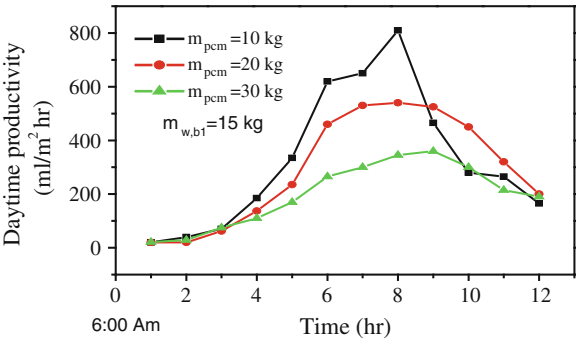

Fig. 2.17 Variation of daytime productivity of NDSS for $m_{pcm} = 10$, 20 and 30 kg with $m_w = 15$ kg

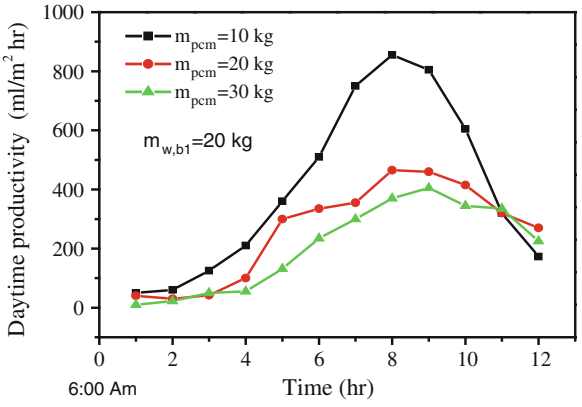

Fig. 2.18 Variation of daytime productivity of NDSS for $m_{pcm} = 10$, 20 and 30 kg with $m_w = 20$ kg

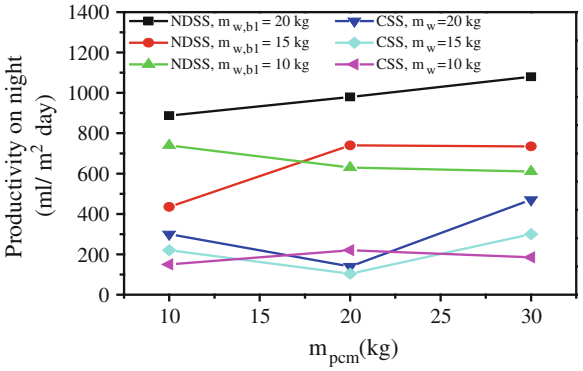

Fig. 2.19 The productivity on night of NDSS and CSS for $m_{pcm} = 10$, 20 and 30 kg with $m_w = 10$, 15 and 20 kg

Table 2.4 The daytime and on night productivity of NDSS of 10, 20 and 30 kg of PCM with 20 kg of water

Mass of PCM kg	Mass of water kg	Productivity on night, kg/m^2 day	Daytime productivity on kg/m^2 day
10	20	887	4.823
20	20	980	3.132
30	20	1,080	2.484

2.339 kg/m^2 day compared with 20 kg of basin1 water with 30 kg of PCM. Thus 10 kg of PCM is suitable for storage system. However the price of 30 kg of PCM is costly if compared with 10 kg of PCM.

2.4.6 Variation of Daily Productivity with Altered Mass of PCM

The daily productivity is represented in Figs. 2.20, 2.21 and 2.22. It is clear that the highest productivity within 20 kg of water basin1 with 10 kg of PCM fee Fig. 2.16.

In order to have a comparison, amounts of total productivity of the designed stills and other still configurations are provided in Table 2.5.

2.5 Statistical Analysis

The productivity of NDSS was optimized using response surface methodology (RSM) provided by STATISTICA 8 software. A standard RSM design tool known as Central Composite Design (CCD) was applied to study the parameters affecting the performance of NDSS. The central composite experimental design (CCD) is a

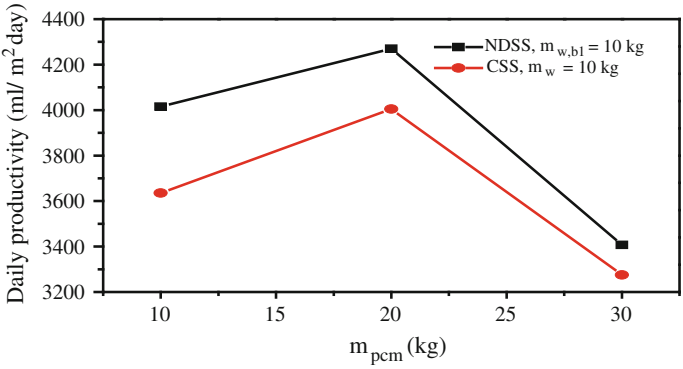

Fig. 2.20 Variation of daily productivity of NDSS with CSS for $m_{w,b1} = 10$ kg, $m_{pcm} = 10$, 20 and 30 kg and $m_w = 10$ kg

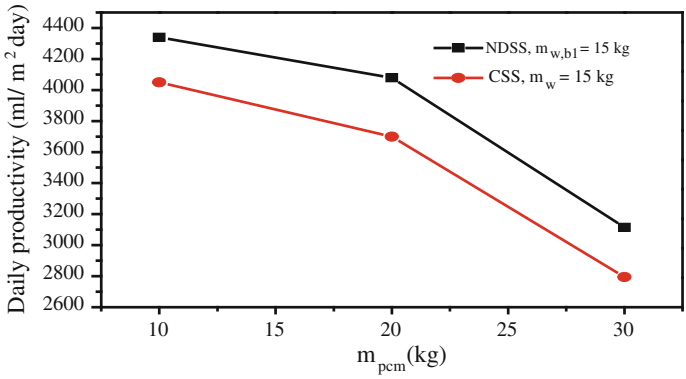

Fig. 2.21 Variation of daily productivity of NDSS with CSS for $m_{w,b1} = 15$ kg, $m_{pcm} = 10$, 20 and 30 kg and $m_w = 15$ kg

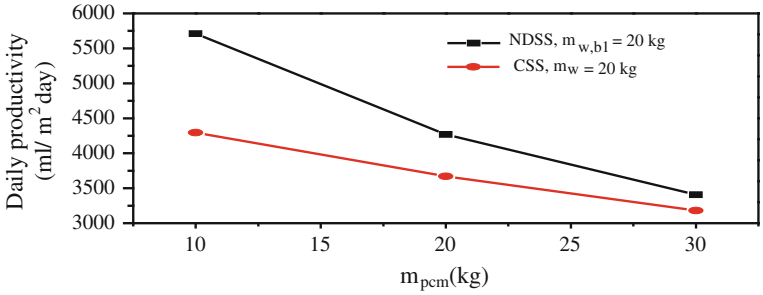

Fig. 2.22 Variation of daily productivity of NDSS with CSS for $m_{w,b1} = 20$ kg, $m_{pcm} = 10$, 20 and 30 kg and $m_w = 20$ kg

Table 2.5 Comparison between total productivity of the designed still and other still configurations

Still type	Date	Productivity (kg/m^2 day)
Designed NDSS (present work)	08/06/2012	5.71
Designed still with LHTESS [26]	23/05/2009	4.85
Designed still with a separate condenser [26]	2009	4.59
Inclined type with black fleece [12]	May, 2004	2.995
Basin type only [27]	16/08/2006	1.88
Basin type with sponge [27]	13/08/2006	2.26
Basin type with wick [27]	06/04/2006	4.07
Basin type with fin [27]	28/08/2006	2.81

Table 2.6 Independent variables and levels used for experimental design

Independent variables	Codes	Variable levels		
		−1	0	+1
Temperature difference between water and glass cover (°C)	X_1	6	13	20
Ambient temperature (°C)	X_2	20	35	50
Solar radiation W/m^2	X_3	260	630	1,000

suitable design for sequential experiments to obtain appropriate information for testing lack of fit (Table 2.6).

2.5.1 Optimization of Parameters

The response surface methodology was used for the optimization of parameters. Among the models that can be fitted to the response (linear, two factor interaction (2FI) and quadratic polynomial), the quadratic model was selected as it is the best model due to its highest order polynomial with significance of additional terms. The model equation based on the coded values (X_1, X_2 and X_3 as temperature difference between water and glass cover, ambient temperature and solar radiation respectively) for the productivity of NDSS was expressed by Equation below.

$$Y = 378.97 + 84.99X_1 - 50.65X_1^2 + 38.7X_2 - 31.9X_2^2 + 171.1X_3 - 18.7X_3^2 - 6.8X_1X_2 + 30.6X_1X_3$$

The result of statistical analysis of variance (ANOVA) was carried out to determine the significance and fitness of the quadratic model as well as the effect of significant individual terms and their interaction on the chosen responses. The p value (probability of error value) is used as a tool to check the significance of each regression coefficient, which also indicates the interaction effect of each cross product. The smaller the p-value, the bigger is the significance of the corresponding coefficient [28] In the case of model terms, the p-values less than 0.05

indicated that the particular model term was statistically significant. From the ANOVA results, the main model terms suggested that variables with significant influence on productivity of NDSS response were temperature difference between water and glass cover (X_1) ambient temperature (X_2), solar radiation (X_3), and the interaction terms were found to exist between the main factors (X_1 X_2 and X_1 X_3), while the significant quadratic terms were temperature difference between water and glass cover (X_1^2), ambient temperature (X_2^2) and solar radiation (X_3^2). The lack of fit test with p-value of 0.0521, which is not significant (p-value > 0.05 is not significant) showed that the model satisfactorily fitted to experimental data. Insignificant lack of fit is most wanted as significant lack of fit indicates that there might be contribution in the regress or-response relationship that is not accounted for by the model [38]. The predicted values versus actual values for productivity of NDSS with adjusted R^2 value of 0.95 indicated that the predicted values and experimental values were in reasonable agreement Fig. 2.23. It means that the data fit well with the model and give a convincingly good estimate of response for the system in the range studied. The developed second-order regression model is complex with many variables. It is difficult to understand the effect of different independent variables from the regression model, but graphical representations are easier to interpret. Contour and response surface plots were drawn (not shown in the paper) to observe the effect of solar radiation, ambient temperature, difference temperature of water and glass on productivity of NDSS. These plots were generated by holding one of the variables at its mid-point and varying the other two variables to obtain the response. The elliptical shape of the curves indicated a strong interaction between the variables. Therefore, it is concluded that the generated model showed reasonable predictability and sufficient accuracy for the productivity of NDSS in the experimental conditions used.

2.6 Conclusions

Two solar stills, NDSS and CSS were constructed for comparing the performance of the stills productivity in sunny and cloudy days. The effect of mass water and mass of PCM were also investigated on the total productivity of stills. The experiments were conducted in typical days under weather conditions of Varanasi, India. The concluded results are presented as follows:

Using integrated condenser will reduce the glass temperature. The saline water in basin1 and basin 2 will also be heated and evaporated to increase the productivity of the solar still because the temperature of integrated condenser is lower than evaporator. The shielded condenser will keep the outer wall of condenser cool. To get benefit from circulation of the water vapor inside integrated condenser, the stepped basin 2 is housed in the condenser from left and right side and free from other side to let the mixture to circulate.

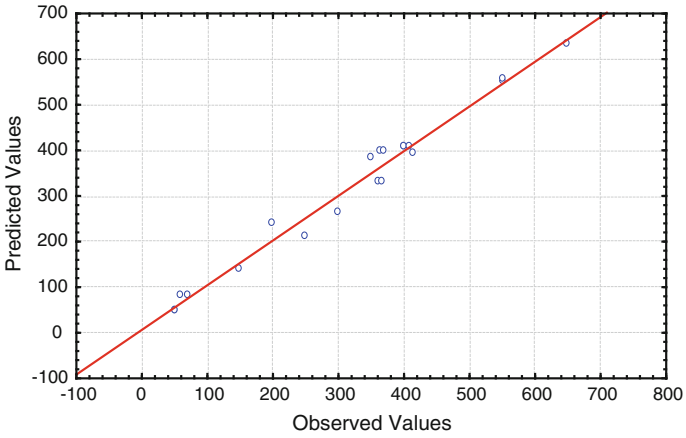

Fig. 2.23 Predicted versus experimental productivity of NDSS

- The daily productivity of NDSS is slightly higher than the CSS in all days 5.71 kg/m^2 day for NDSS and 4.295 kg/m^2 day for CSS. Thus, NDSS is favored for sunny and partially cloudy days due to the higher productivity.
- The productivity during night time of NDSS is mostly higher than the CSS in all days. This increase is due to the increase of the mass of PCM. Thus it is necessary to consider using it in solar still system. Furthermore, the transferred heat from the PCM to the saline water during discharge process is enough to produce high amount of distillated water because of decreasing in operating temperature which is compared with low ambient temperature at night condition.

Appendix

Acronyms

SSWLA	Solar still with lauric acid
SSWMA	Solar still with myristic acid
LA	Lauric Acid
MA	Myristic Acid
UNEP	United Nations Environment Programme
WHO	World Health Organization
WMO	World Meteorological Organization

Nomenclature

A	Area, m^2
C_p	Specific heat, J/kg °K
dt	Time interval, s

Gr Grashof number
h Heat transfer coefficient, W/m^2 °K
h_{cw} Convective heat transfer coefficient from water surface to the glass cover, W/m^2 °K
h_{ew} Evaporative heat transfer coefficient from water surface to the glass cover, W/m^2 °K
h_{rw} Radiative heat transfer coefficient from water surface to the glass cover, W/m^2 °K
h_1 Total heat transfer coefficient from water to glass cover, W/m^2 °K
h_2 Convective heat transfer coefficient from glass to ambient, W/m^2 °K
h_3 Convective heat transfer coefficient from basin liner to water, W/m^2 °K
i Current, ampere
$I(t)$ Solar flux on an inclined collector, W/m^2
m Mass, kg
mew Productivity, ml/m^{2}hr
P Partial pressure, N/m^2
Pr Prandtl number
q Heat transfer, W/m^2
Ra Rayleigh number
T Temperature, °C
U_{ga} Overall heat transfer coefficient from inner glass to ambient, W/m^2
U_b Overall bottom loss coefficient, W/m^2
U_t Top loss coefficient, W/m^2
U_L Overall heat transfer coefficient, W/m^2
K Thermal conductivity, W/mK
L,x Thickness, m
l Liquid
s Solid
v Wind speed, m/s

Greek symbols
α Absorptivity
α' Fraction of solar energy absorbed
ε Emissivity
δ Incremental rise, °K
σ Stefan-Boltzmann constant, W/m^2 °K^4
τ Transmittance coefficient
η_i Instantaneous efficiency (%)
ΔT Effective temperature difference (°K)
γ Latent heat of vaporization J/kg

Subscripts
a Ambient
b Basin
c Convective

cond	Conduction
e	Evaporative
eff	Effective
f	Film temperature
g	Glass
in	Inner
ins	Insulation
mt	Melting
o	Outer
pcm	Phase change material
r	Radiation
w	Water

References

1. Shukla SK, Sorayan VPS, Gupta SK (2004) Parametric studies of passive/active solar stills by using modified convective mass transfer relations. Int J Ambient Energy 25(3):212–232
2. Shukla SK (2003) Computer modeling of passive solar still by evaluating absorptivity of the basin liner. Int J Ambient Energy 243:123–132
3. Malik MAS, Tiwari GN, Kumar A, Sodha MS (eds) (1982) Solar distillation a practical study of a wide rang of stills and their optimum design, construction and performance. Pergamon Press, New York
4. Fath H (1998) Solar distillation: a promising alternative for water provision with free energy, a simple technology and a clean environment. Desalination 116:45–56
5. Dunkle RV (1961) Solar water distillation: the roof of type still and multiple effect diffusion still, international developments in heat transfer. In: A.S.M.E, Proceeding of International Heat Transfer, part V, University of Colorado, p 895
6. Cooper PI (1973) Digital simulation of experimental solar still data. Sol Energy 14:451
7. Abdallaha S, Abu-Khader MM, Badran B (2009) Effect of various absorbing materials on the thermal performance of solar stills. Desalination 242:128–137
8. Abdulhaiy MR (2005) Transient performance of a stepped solar still with built-in latent heat thermal energy storage. Desalination 171(1):61–76
9. Agyenim F, Eames P, Smyth M (2009) A comparison of heat transfer enhancement in a medium temperature thermal energy storage heat exchanger using fins. Sol Energy 83(9):1509–1520
10. El-Bahi A, Inan D (1999) Analysis of a parallel double glass solar still with separate condenser. Renew Energy 17(4):509–521
11. Al-Hamadani AAF, Shukla SK (2011) Water distillation using solar energy system with lauric acid as storage medium. Int J Energy Eng 1(1):1–8
12. Aybar HŞ, Egelioğlu F, Atikol U (2005) An experimental study on an inclined solar water distillation system. Desalination 180(1–3):285–289
13. Dwivedi VK, Tiwari GN (2009) Comparison of internal heat transfer coefficients in passive solar stills by different thermal models: an experimental validation. Desalination 246(1–3):304–318
14. El-Sebaii AA, Al-Ghamdi AA, Al-Hazmi FS, Faidah AS (2009) Thermal performance of a single basin solar still with PCM as a storage medium. Appl Energy 86(7–8):1187–1195

15. El-Swify ME, Metias MZ (2002) Performance of double exposure solar still. Renew Energy 26(4):531–547
16. Fath HES, Elsherbiny SM (1993) Effect of adding a passive condenser on solar still performance. Energy Convers Manage 34(1):63–72
17. Fath HES, Hosny HM (2002) Thermal performance of a single-sloped basin still with an inherent built-in additional condenser. Desalination 142(1):19–27
18. Garg HP, Mann HS (1976) Effect of climatic, operational, and design parameters on the year round performance of single-sloped and double-sloped solar still under Indian arid zone conditions. Sol Energy (United States) 18(2):159–164 (Medium: X)
19. Kalogirou S (2009) Solar energy engineering: processes and systems, 1st edn. Academic Press is an imprint of Elsevier, USA
20. Lacroix M, Benmadda M (1997) Numerical simulation of natural convection-dominated melting and solidification from a finned vertical wall. Numer Heat Transf, Part A: Appl 31(1):71–86
21. Madhlopa A (2009) Development of an advanced passive solar still with separate condenser Ph.D. Strathclyde, Glasgow
22. Madhlopa A, Johnstone C (2009) Numerical study of a passive solar still with separate condenser. Renew Energy 34(7):1668–1677
23. Maroo SC, Goswami DY (2009) Theoretical analysis of a single-stage and two-stage solar driven flash desalination system based on passive vacuum generation. Desalination 249(2):635–646
24. Naim MM, El-Kawi MAA (2002) Non-conventional solar stills Part 2. Non-conventional solar stills with energy storage element. Desalination 153(1–3):71–80
25. Noordin MY, Venkatesh VC, Sharif S, Elting S, Abdullah A (2004) Application of response surface methodology in describing the performance of coated carbide tools when turning AISI 1045 steel. J Mater Process Technol 145:46–58
26. Tabrizi FF, Dashtban M, Moghaddam H (2010) Experimental investigation of a weir-type cascade solar still with built-in latent heat thermal energy storage system. Desalination 260(1–3):248–253
27. Velmurugan V, Gopalakrishnan M, Raghu R, Srithar K (2008) Single basin solar still with fin for enhancing productivity. Energy Convers Manage 49(10):2602–2608
28. Sarı A, Kaygusuz K (2002) Thermal and heat transfer characteristics in a latent heat storage system using lauric acid. Energy Convers Manage 43(18):2493–2507
29. Montgomery DC (2001) Design and analysis of experiments, 5th edn. Wiley, New York
30. Myers RH, Montgomery D (2000) Response surface methodology: process and product optimization using designed experiments, 2nd edn. Wiley, USA
31. Nafey AS, Abdelkader M, Abdelmotalip A, Mabrouk AA (2002) Enhancement of solar still productivity using floating perforated black plate. Energy Convers Manage 43(7):937–946
32. Sarı A (2003) Thermal reliability test of some fatty acids as PCMs used for solar thermal latent heat storage applications. Energy Convers Manage 44(14):2277–2287
33. Shukla SK, Sorayan VPS (2005) Thermal modeling of solar stills: an experimental validation: renewable Energy. Fuel Energy Abstr 30(5):683–699

http://www.springer.com/978-3-642-45175-1

Modern Mechanical Engineering
Research, Development and Education
Davim, J.P. (Ed.)
2014, VIII, 466 p. 360 illus., Hardcover
ISBN: 978-3-642-45175-1